Plasma Catalysis for CO_2 Hydrogenation: Unlocking New Pathways Towards CH_3OH

Roel Michiels, Yannick Engelmann and Annemie Bogaerts*
Research group PLASMANT, University of Antwerp, Department of Chemistry
Universiteitsplein 1, BE-2610 Wilrijk-Antwerp, Belgium

*: annemie.bogaerts@uantwerpen.be

Abstract

We developed a microkinetic model to reveal the effects of plasma-generated radicals, intermediates and vibrationally excited species on the catalytic hydrogenation of CO_2 to CH_3OH on a Cu(111) surface. As a benchmark, we first present the mechanisms of thermal catalytic CH_3OH formation. Our model predicts that the RWGS reaction followed by CO hydrogenation, together with the formate path, mainly contribute to CH_3OH formation in thermal catalysis. Adding plasma-generated radicals and intermediates results in a higher CH_3OH turnover frequency (TOF) by six to seven orders of magnitude, showing the potential of plasma-catalytic CO_2 hydrogenation into CH_3OH, in accordance with literature. In addition, CO_2 vibrational excitation further increases the CH_3OH TOF, but the effect is limited, due to relatively low vibrational temperatures under typical plasma catalysis conditions. The predicted rise in CH_3OH formation by plasma catalysis is mainly attributed to the increased importance of the formate path. In addition, the conversion of plasma-generated CO to HCO* and subsequent HCOO* or H_2CO* formation contribute to CH_3OH formation. Both pathways bypass the HCOO* formation from CO_2, which is the main bottleneck in the process. Hence, our model points towards the important role of CO, but also O, OH and H radicals, as they influence the reactions that consume CO_2 and CO. In addition, our model reveals that the H pressure should not be smaller than ca. half of the O pressure in the plasma, as this would cause O* poisoning, which would result in very small product TOFs. Thus, plasma conditions should be targeted with a high CO and H content, as this is favourable for CH_3OH formation, while the O content should be minimized.

Keywords

Catalytic CO_2 hydrogenation into CH_3OH, plasma catalysis, thermal catalysis, microkinetic modeling, pathways

1. Introduction

There is growing interest into various strategies to convert CO_2 into high-value chemicals. This is challenging as CO_2 is a molecule with high thermodynamic stability. An interesting route is hydrogenation to methanol (CH_3OH), which has a lower thermodynamic limitation than direct CO_2 decomposition and dry reforming of methane (DRM).[1,2] From a thermodynamic perspective, CO_2/H_2 conversion into CH_4 (methanation process) is preferred at low temperature (< 900 K), while conversion into CO and H_2O (reverse water-gas shift (RWGS) reaction) is preferred at high temperature (> 900 K). However, the direct production of CH_3OH from CO_2 hydrogenation would be desirable, because CH_3OH is a valuable fuel and chemical intermediate. The book 'Methanol Economy' written by Nobel Prize winner George Andrew Olah, proposes CH_3OH as a key solar fuel in the anthropogenic energy cycle.[3]

At room temperature and ambient pressure, the equilibrium gas phase CH_3OH yield from CO_2/H_2 is near 0 % and CH_3OH production processes (from syngas or) from CO_2 are therefore operating at increased pressure, which is favorable due to the stoichiometry of the reaction. Thermodynamically, the process also benefits from lower operating temperature due to the exothermicity of the process

(-50 kJ/mol). However, this is kinetically unfavorable because of the high dissociation barrier of CO_2 that needs to be overcome. A compromise is made by operating at ~200 °C and 50 bar.[4]

A possible solution could be the combination of catalysis with non-thermal plasma, which offers a unique way to enable kinetically limited processes, while maintaining thermodynamically favorable temperatures.[5–7] In non-thermal plasma, highly energetic electrons can produce excited and reactive species through inelastic collisions with feedstock molecules, promoting the (rate-limiting) dissociation of CO_2.[5,8] To overcome the low yields at ambient pressure, both experimental and computational studies have suggested that separation of CH_3OH from the gas phase, by cooling into liquid phase, can shift the chemical equilibrium.[9–11]

In general, plasma catalysis has the potential to bypass slow reaction steps in thermal catalysis through reactive gas phase processes in the plasma, and to improve the selectivity towards desired products compared to plasma alone due to the presence of a catalyst. Synergistic plasma-catalyst interactions contribute in different ways to enhancing the conversion, product yield and energy efficiency of the process, as well as enhancing the catalyst stability, by reducing poisoning, coking and sintering.[5,8,12]

Plasma-catalytic CO_2 hydrogenation into CH_3OH has recently attracted interest by several authors. Eliasson et al.[13] investigated the hydrogenation of CO_2 to CH_3OH in a dielectric barrier discharge (DBD) plasma, both with and without the presence of a $CuO/ZnO/Al_2O_3$ catalyst for a 3:1 H_2/CO_2 ratio. They reported CO and H_2O as major products for the plasma-only case. Other components detected were CH_4 and CH_3OH, with a selectivity of 3-4 % and 0.4-0.5 %, respectively. Adding the catalyst resulted in a 10 times and 10-20 times increase in CH_3OH yield and selectivity, respectively. Optimizing the system to use low power and high pressure further enhanced the CH_3OH selectivity over CH_4. The maximum CH_3OH yield was however still low, i.e. ~1 %. More recently, Zeng and Tu[14] studied CO_2 hydrogenation in a DBD plasma at low temperatures and atmospheric pressure with and without catalyst, i.e. $Cu/\gamma\text{-}Al_2O_3$, $Mn/\gamma\text{-}Al_2O_3$ and $Cu\text{-}Mn/\ \gamma\text{-}Al_2O_3$. Without catalyst, the conversion was found to be 7.5 % and the main products were CO and CH_4 with 46 % and 8 % selectivity, respectively. Adding the catalyst increased the CO_2 conversion to 8-10 % and the CO selectivity and yield to 76-80 % and 6.4-7.9 %, respectively. No CH_3OH was detected but this might have been due to the inability of their gas chromatography setup to detect this compound. Parastaev et al.,[15] investigated plasma-catalytic hydrogenation of CO_2 on a $Cu/CeZrO_4$ catalyst, again in a DBD plasma, with a temperature-programmed plasma surface reaction method. They reported that the hydrogenation is mostly selective towards CO and CH_4, while CH_3OH formation was not monitored. Finally, Wang et al.,[16] reported a relatively high CH_3OH yield and selectivity of 11.3 % and 53.7 %, respectively. These values were achieved under conditions of atmospheric pressure and room temperature, using a DBD plasma reactor with water electrode and packed with a $Cu/\gamma\text{-}Al_2O_3$ catalyst. The high selectivity was attributed to the water electrode that removes CH_3OH from the gas phase, thereby shifting the chemical equilibrium. Other reasons for why the water electrode enhances the methanol selectivity, as suggested by Liu et al.,[17] are a low temperature due to cooling and different discharge properties. Wang et al., also reported an enhanced selectivity towards CH_3OH, even without the use of the water electrode. One of the possible causes of this effect was suggested to be the formation of CO in the gas phase and the subsequent hydrogenation at the surface. Furthermore, they concluded that the reactor geometry had an important effect, while the H_2/CO_2 ratio was found to be of little importance. Although clearly more research is needed, these studies show that plasma-catalytic CO_2 hydrogenation over a Cu catalyst might have the potential to sustainably produce CH_3OH at low temperature and atmospheric pressure.

In spite of the growing interest in plasma-catalytic CO_2 hydrogenation, the underlying reaction mechanisms are still unclear. Thermal catalytic CO_2 hydrogenation has been studied computationally by several authors, as outlined in more detail in the next section. However, the situation in plasma catalysis is much more complex, because of the unknown behavior and relative impact of various

plasma components (i.e., radicals, ions, vibrationally and electronically excited species, and electrons, as well as the electric field) at the catalyst surface. Therefore, computational modeling to study their behavior is crucial for further advancement in the field of plasma catalysis and optimization of the plasma-catalytic CO_2 hydrogenation.

Only a few authors have attempted to describe the effects of plasma species at a catalyst surface. Bal, Jafarzadeh et al., applied density functional theory (DFT) to study the effect of surface charging on CO_2 activation on supported M/Al_2O_3 (M = Ti, Ni, Cu) single atom catalysts[18] and on TiO_2-supported Cu_5 and Ni_5 nanoclusters[19], as well as the synergy between electric field, surface morphology and excess electrons on Cu surfaces.[20] In addition, Bal et al. developed a method to simulate chemical reactions under vibrational non-equilibrium.[21]

Plasma indeed produces vibrationally excited species, and some authors have studied to which degree vibrational excitation of a specific normal mode lowers the activation barrier of specific surface reactions, albeit not directly in the context of plasma catalysis. The effect of the different vibrational modes is well-known for CH_4. For instance, Juurlink et al.,[22] found that both C – H stretching excitation and bending excitation activate CH_4 dissociation on Ni(111) and Ni(100). The former mode is generally more efficient. Furthermore, they reported that the surface morphology and metal can determine the efficacy of the vibrational modes. For CO_2, the impact of vibrational excitation and mode specificity is less clear. Jiang et al.,[23] reported that vibrational excitation enhances dissociative adsorption of CO_2 on Ni(100) and that the asymmetric stretching mode is most efficient, followed by the symmetric stretch and bending mode. Similarly, Farjamnia et al.,[24] reported that CO_2 dissociation on Ni(100) is enhanced by vibrational excitation of CO_2, based on DFT calculations. Recently, Quan et al.,[25] reported that HCOO* formation on Cu(111) and Cu(100) from CO_2 and H_2 was enhanced by the bending excitation of CO_2. They found that the transition state has a significantly smaller OCO angle, with energy supplied from the bending mode. Their findings were based on both calculations and molecular beam experiments. Their results are quite remarkable as they find vibrational excitation to enhance bond formation, not dissociation.

In addition, plasma generates a wide variety of radicals in high concentrations, and they can largely impact the catalytic mechanisms. There exist a few kinetic models studying the impact of plasma species, starting from traditional thermal catalytic mechanisms. Mehta et al.,[26] developed a microkinetic model for NH_3 synthesis to study the impact of N_2 vibrational excitation on reaction rates, starting from a thermal catalysis microkinetic model. They reported that the plasma-catalyst combination can produce NH_3 at conditions inaccessible for thermal catalysis, as observed in experiments. They also predicted a shift in the optimal catalyst material, i.e. the volcano plot shifted horizontally, to a lower metal-N* binding energy, i.e. more noble catalysts. Besides the horizontal shift, the volcano plot also shifted vertically to higher rates. In another paper,[27] they showed that plasma catalysis can surpass the thermodynamic conversion limit, because non-thermally activated reaction channels can kinetically trap the produced NH_3. A similar microkinetic model for NH_3 synthesis was developed by Engelmann et al.,[28] which not only studied the impact of vibrational excitation but also the effect of radicals and Eley-Rideal reactions. In addition, Engelmann et al.,[29] developed a microkinetic model for the non-oxidative coupling of methane, studying the effect of both vibrational excitation and radicals. Like Mehta et al., a horizontal and vertical shift of the volcano plot was predicted due to vibrational excitation. The plasma radicals affect the rates and selectivity differently, depending on the catalyst material. Catalysts that exhibit stronger binding are less impacted by changes in the gas phase species, as product formation rates are low due to poisoning of the catalyst surface and low desorption rates, while more noble catalysts benefit greatly from the presence of radicals in the gas phase that efficiently recombine at the catalyst surface.

To our knowledge, however, no model has been developed yet to describe plasma-catalytic CO_2 hydrogenation into CH_3OH, and – as illustrated in the next section – even for thermal catalytic CO_2 hydrogenation into CH_3OH, there is no consensus yet on the important mechanisms. Therefore, the

aim of this paper is to compare the pathways of thermal catalytic and plasma-catalytic CO_2 hydrogenation into CH_3OH, by means of a microkinetic model. More specifically, we want to examine whether reactive plasma species can avoid the steep activation barriers in thermal catalysis**,** and give rise to more favorable reaction pathways for CO_2 hydrogenation into CH_3OH. We will focus on vibrationally excited species and reactive plasma species, interacting with a Cu(111) catalyst, which is mostly used for this application in thermal catalysis.[30,31]

2. Catalytic pathways of CO_2 hydrogenation to CH_3OH on Cu: State-of-the-art and potential benefits of plasma catalysis

To study plasma-catalytic hydrogenation of CO_2 into CH_3OH on Cu, first the thermal catalytic process has to be understood, in order to investigate the influence of the plasma species on the surface chemistry. Hence, we will first review the mechanisms of thermal catalytic CO_2 hydrogenation into CH_3OH, as revealed by kinetic studies in literature, based on DFT calculations.

The very first studies supported a formate route where CO_2 was first hydrogenated to formate (HCOO*) followed by subsequent hydrogenation to dioxymethylene (H_2COO*), formaldehyde (H_2CO*) and methoxy (H_3CO*). However, only HCOO* and H_3CO* were observed.[32] Grabow et al.,[30] constructed a mean-field microkinetic model that was fitted with experimental results obtained on a $Cu/ZnO/Al_2O_3$ (CZA) catalyst. They included formic acid (HCOOH*) and H_2COOH* in their calculations and proposed a formate route where HCOO* was preferentially hydrogenated to HCOOH* instead of H_2COO*. HCOOH* was then further hydrogenated to H_2COOH* which splits into H_2CO* and OH*. Finally, H_2CO* was further hydrogenated. Yang et al.,[33] performed reactivity studies and DFT calculations showing that CH_3OH synthesis on Cu surfaces proceeds through a HCOO* intermediate to H_2CO*, but via H_2COO* instead of HCOOH*. The overall reaction rate was found limited by both HCOO* and H_2COO* hydrogenation. Kattel et al.,[34] reported the transformation of CO_2 to CH_3OH via HCOO*, HCOOH*, H_2COOH*, and H_3CO* intermediates based on spectroscopic studies and both DFT and kinetic Monte Carlo (kMC) simulations. Contrary to the formate route, Zhao et al.,[31] found that CO_2 hydrogenation proceeds through a hydrocarboxyl (COOH*) route that is kinetically more favourable in the presence of water via a unique hydrogen transfer mechanism. This is rather remarkable as H_2O is generally considered a poison through OH* formation. They found that hydrogenation through HCOO* on a Cu(111) surface was not feasible because of the high activation barriers in some steps. The authors only based their conclusions on DFT data, but their findings were supported by experiments conducted by Yang et al.[35]

Besides the formate and hydrocarboxyl path, a reverse water-gas shift (RWGS) reaction followed by CO hydrogenation is also a possible mechanism. However, it is hitherto uncertain whether CO hydrogenation to CH_3OH is kinetically possible. Indeed, in the industrial CH_3OH production from syngas, CO_2 is added to keep the CZA catalysts oxidized, but research shows that under such circumstances, CO_2 is the sole carbon source for CH_3OH.[1,2,36] For instance, Grabow et al.,[30] proposed that on Cu (111) both CO and CO_2 hydrogenation are possible. Yang et al.[33] on the other hand, found that on Cu surfaces the RWGS reaction only leads to CO desorption, because further hydrogenation stops at HCO*, which decomposes back into CO*. Zhao et al.,[31] also concluded that the RWGS mechanism was less important on Cu(111) than the hydrocarboxyl path. Studt et al.,[36] conducted experiments and constructed a microkinetic model, paying special attention to the effect of ZnO promoted Cu. They found that on Cu/MgO, which behaves similar to Cu(111), CO hydrogenation was blocked because of high formate coverage on the surface. ZnO was proposed to increase binding to O-bound intermediates, thereby increasing the rate of CO_2 hydrogenation.

Clearly, there is no consensus yet on the main thermal catalytic CH_3OH formation mechanisms from CO_2 hydrogenation. A summary of all proposed pathways is presented in Figure 1.[1] Three possible

mechanisms can be distinguished, i.e. the formate route (green path in Figure 1), the hydrocarboxyl route (yellow path) and the RWGS reaction followed by CO hydrogenation (blue path). Which mechanism is most important will depend on the specific gas phase composition, catalyst characteristics and process conditions .

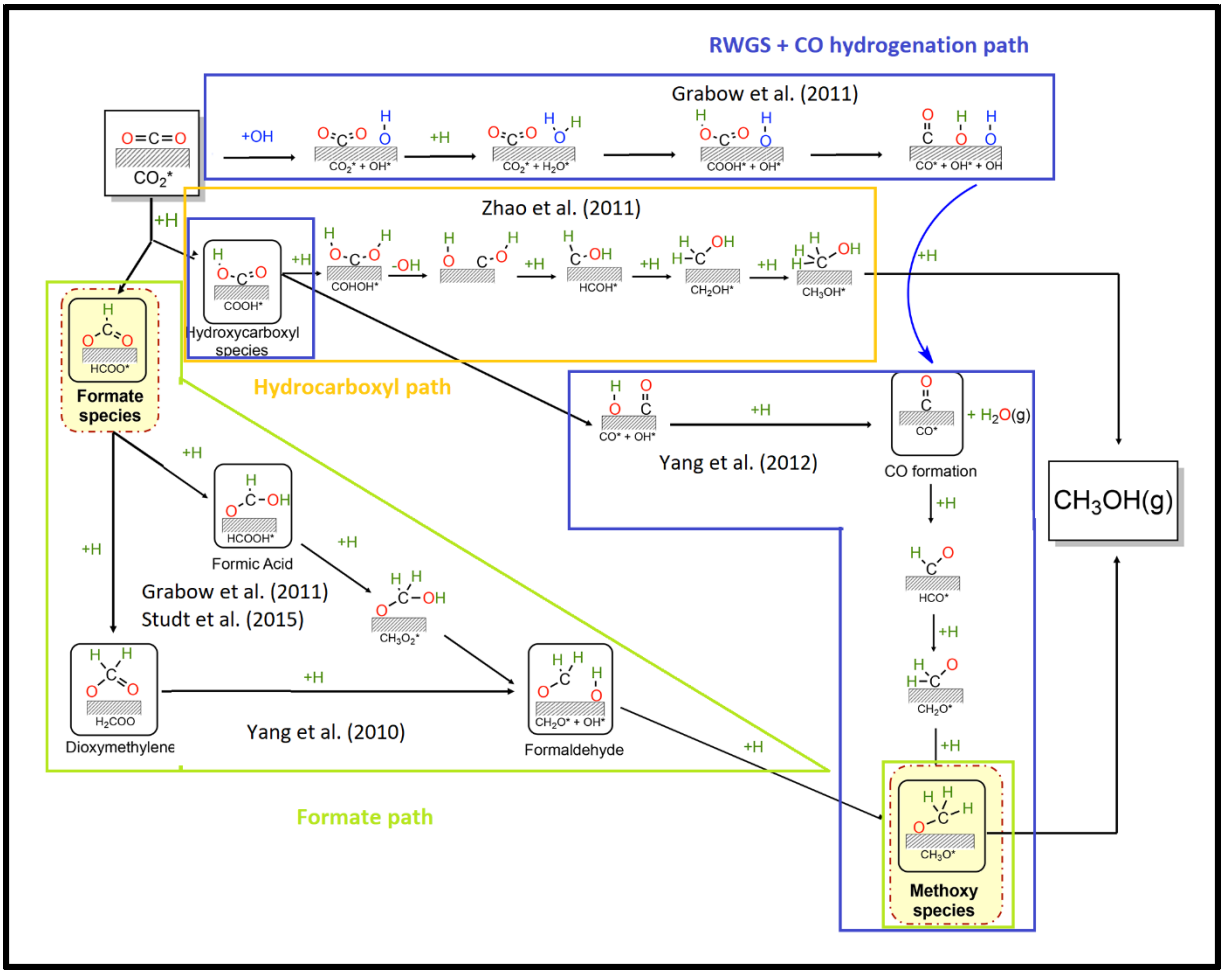

Figure 1: Three possible pathways for thermal catalytic CO_2 hydrogenation into CH_3OH: (i) the formate pathway, through HCOO* and subsequently HCOOH* or H_2COO* (in green), (ii) the hydrocarboxyl pathway through COOH* and COHOH* (yellow path), and (iii) the RWGS reaction followed by CO hydrogenation (blue path). The RWGS reaction depicted on the figure goes through COOH* or CO is formed with the help of an OH* species. CO can also be formed from HCOO*, which is not depicted. Adapted from Alvarez et al.[1]

A central question in plasma-catalytic CO_2 hydrogenation is how the plasma affects the aforementioned pathways and thereby impacts the CH_3OH production rate. Indeed, we may expect that the plasma will be able to bypass certain steps of thermal catalysis, which have a high energy barrier, as depicted in Figure 2. For instance, Zhao et al.,[31] suggested the formation of COOH* to be rate-limiting for CH_3OH formation. The plasma might be able to bypass this step via the generation of CO and OH in the gas phase and subsequent association to COOH* on the surface (yellow path in Figure 2). Similarly, CO could recombine with H* at the surface to form HCO* (green path in Figure 2), which bypasses HCOO* hydrogenation and H_2COOH* dissociation, which are both reaction steps that are potentially rate-limiting due to the high energy barrier. While Yang et al.[33] claimed further hydrogenation of HCO* is difficult in thermal catalysis, the hydrogenation is possibly facilitated in plasma catalysis, due to a high density of plasma-generated H radicals. Finally, also vibrational

excitation can enhance CH_3OH formation when it lowers the barrier for a rate-limiting step. For instance, vibrational excitation of CO_2 could lower the barrier for COOH* or HCOO* formation, resulting in a higher rate of CH_3OH formation (purple path in Figure 2).

It is the aim of this paper to elucidate and concretize these possible hypotheses, and formulate how plasma radical and intermediates, and vibrational excitation can impact the plasma-catalytic CO_2 hydrogenation. This is done by means of microkinetic modelling, starting from the thermal catalytic pathways and expanded to include unique plasma pathways.

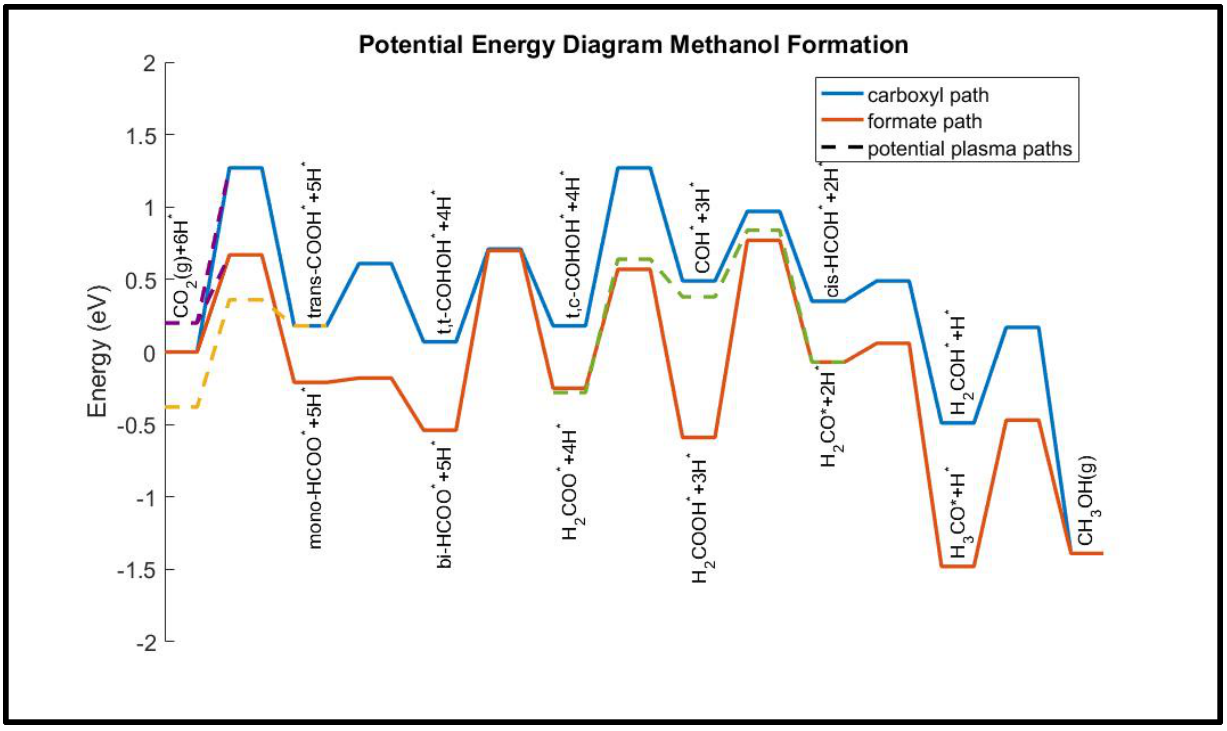

Figure 2: Possible influence of plasma on thermal catalytic pathways for CH_3OH synthesis, adapted from Zhao et al.[31] The RWGS pathway is omitted for clarity. The dashed yellow and green lines indicate how plasma species can bypass certain pathways. Yellow: CO*+OH* → COOH*. Green: CO*+2H* → HCO*+H* → H_2CO*. Purple: lowering of a barrier due to vibrational excitation of CO_2.

3 Methodology

3.1 Microkinetic model

Microkinetic modelling is often used to study mechanisms in catalysis. In short, microkinetic modelling consists of setting up a rate equation for each surface species, based on a set of elementary reactions. As such, microkinetic models make no assumptions regarding the surface coverage of species or the rate-determining step.

We developed a mean-field microkinetic model, similar to Engelmann et al.,[29] for CO_2 hydrogenation into CH_3OH. The mean-field approximation neglects the local topology of the surface and assumes that every compound on the surface can interact with every other compound on the surface. The reaction rates are calculated as:

$$r_j = k_{j,f} \prod_s a_s^{c_{sj,\,f}} - k_{j,b} \prod_s a_s^{c_{sj,\,b}}$$

Where $k_{j,f}$ is the forward and $k_{j,b}$ the backward rate coefficient of the reaction, a_s is the activity of species s and $c_{sj,f}$ and $c_{sj,b}$ are the stoichiometric coefficients of species s in the forward and backward reaction, respectively. For gas phase species the activity is equal to the normalized pressure and for adsorbates it is equal to the surface coverage. The forward rate coefficient is calculated from the Eyring equation, derived from transition state theory (TST):

$$k_f = k_{TST} = \frac{k_B T}{h} e^{\frac{\Delta S^{\ddagger}}{R}} e^{\frac{-\Delta H^{\ddagger}}{RT}}$$

Here, T is the temperature, k_B is the Boltzmann constant, h is Planck's constant and $S^{\ddagger}$ and $H^{\ddagger}$ are the entropy and enthalpy barriers, respectively. The backward rate coefficient is calculated from the forward rate coefficient and K, the equilibrium constant, which is calculated from ΔS_r and ΔH_r, i.e. the reaction entropy and reaction enthalpy:

$$K = e^{\frac{\Delta S_r}{R}} e^{\frac{-\Delta H_r}{RT}}$$

$$k_b = \frac{k_f}{K}$$

This is done to ensure thermodynamic consistency, i.e. $H^{\ddagger}_b = H^{\ddagger}_f - H_r$.

Based on the reaction rates, the time-derivative of the surface coverage for each adsorbate is solved as follows:

$$\frac{\partial \theta_i}{\partial t} = \sum_j c_{ij} . r_j$$

Where θ_i is the surface coverage of adsorbate i, which is defined as the number of adsorbed species of i divided by the number of adsorption sites. Hence, coverages will always lie between zero and one. c_{ij} is the stoichiometric coefficient for adsorbate i in reaction j.

We solved these equations for steady-state coverages, i.e. $_i/\ t = 0$ for all species i. The coverages were then used to calculate steady-state rates and turnover frequencies (TOFs). The TOF is defined as:

$$TOF\ (s^{-1}) = \frac{number\ of\ molecules}{number\ of\ sites\ .\ second} = \frac{coverage}{second}$$

3.2 Reaction set and enthalpy values

The reaction set used in our model, and the corresponding reaction and activation enthalpies, are listed in Table 1. This includes both the reactions of thermal catalysis, and the extra reactions added specifically for plasma catalysis; the latter are indicated with * (i.e., reactions 25, 27 and 47-54). The calculation of the entropies is described in the next section. The reaction set was based on Zhao et al.,[31] as this is the only reaction set reported in literature that includes the hydrocarboxyl path. However, some complementary reactions were added:

R1, R19, R21, R25, R32, R44, R47, R48, R51-54: Adsorption reactions were not reported by Zhao et al.[31] However, they reported surface binding energies. Hence, these energies were taken as reaction enthalpies and adsorption was assumed to have no enthalpic barrier. The radical-adsorption (and also Eley-Rideal (ER)) reactions as implemented in the model assume that the surface is 100% effective in dissipating adsorption energy, i.e., perfect third body, effectively cooling and concentrating the radicals. The adsorption energies for R47 and R48 are taken from Xu et al.,[37] because they were not reported by Zhao et al. This is due to the fact that CH_2 and CH_3 normally do not occur in thermal catalytic methanol synthesis, however they need to be accounted for, as they occur in plasma.
R2 and R3 were taken from Grabow et al.[30] R2, i.e. formate formation from CO_2*, was not reported by Zhao et al., which was motivated by weak CO_2 adsorption. However, as hydrocarboxyl formation from CO_2* was allowed, it seems logical to allow formate formation and CO_2 dissociation as well.
R44-46 were added to prevent unrealistic results when including O radicals coming from the plasma. The energy values were taken from the Catapp database.[38]
R43 was added, as dissociative adsorption of CO_2 might become important due to vibrational excitation of CO_2 by the plasma, and the energies were taken from the Catapp database.
R49 and R50 were added to study the impact of CH_2 and CH_3 radicals from the plasma. Energies were taken from Catapp.

Changes made to reaction enthalpy values found in literature to ensure thermodynamic consistency (i.e. two different routes going from the same reactants to the same products should result in the same overall energy change) are reported in the fifth column of Table 1. The listed reaction enthalpies are the corrected values.

We note that the listed data is based on DFT calculations, which are known to overestimate the adsorption energy of CO (R25 in Table 1). A recent work by Zhao et al., showed that overestimation of CO adsorption energy can lead to non-physical kinetics, such as small free surface and negative CO reaction order.[39] To account for this limitation, we also ran the model using the experimental adsorption energy of CO. The results are presented in the SI (section S.3).

Table 1: Overview of the reactions in the model and the corresponding energy values ($\Delta H^{\ddagger}$: activation enthalpy, ΔH_r: reaction enthalpy, δ: change in reaction enthalpy, to ensure thermodynamic consistency; see text). The small letter in front of a surface species indicates the configuration at the surface (m: mono, b: bis, t: trans, c: cis). An * behind the reaction number indicates reactions that are only in the model for plasma catalysis. When the reaction number is followed by ^{vib}, the impact of vibrational excitation on this reaction is investigated (see sections 3.4 and 4.3).

Reaction number	Reaction	$\Delta H^{\ddagger}$ (eV)	ΔH_r (eV)	δ (eV)
0^{vib}	$H_2(g) + 2* \rightarrow 2H*$	0.60	-0.39	/
1	$CO_2(g) + * \rightarrow CO_2*$	0.00	-0.05	/
2	$CO_2* \rightarrow CO* + O*$	1.77	0.48	1.13
3	$CO_2* + H* \rightarrow mHCOO* + *$	0.87	-0.16	0.09
4	$CO_2* + H* \rightarrow tCOOH* + *$	0.91	0.23	0.47
5^{vib}	$CO_2(g) + H* \rightarrow mHCOO* + *$	0.67	-0.21	/

6	mHCOO* → bHCOO*	0.03	-0.33	/
7	mHCOO* + H* → H_2COO*	1.24	0.29	/
8	H_2COO* + H* → H_2COOH* + *	0.82	-0.34	/
9	H_2COOH* + * → H_2CO* + OH*	1.36	0.52	/
10	H_2CO* + H* → H_3CO* + *	0.13	-1.41	/
11	CH_3OH(g) + 2* → H_3CO* + H*	0.92	-0.09	0.03
12^{vib}	CO_2(g) + H* → tCOOH*	1.27	0.18	/
13	tCOOH* + H* → t,tCOHOH*	0.43	-0.11	/
14	t,tCOHOH* → t,cCOHOH*	0.64	0.11	/
15	t,cCOHOH* + * → COH* + OH*	1.09	0.31	/
16	COH* + H* → HCOH* + *	0.48	-0.14	
17	HCOH* + H* → H_2COH* + *	0.14	-0.84	
18	CH_3OH(g) + 2* → H_2COH* + H*	1.56	0.90	/
19	H_2CO(g) + * → H_2CO*	0.00	-0.12	/
20	bHCOO* + H* → HCOOH* + *	0.81	0.20	/
21	HCOOH(g) + * → HCOOH*	0.00	-0.24	/
22	HCOOH* + H* → H_2COOH* + *	0.90	-0.25	0.07
23	tCOOH* → cCOOH*	0.53	0.03	/
24	cCOOH* → CO* + OH*	0.18	-0.47	0.09
25*	CO(g) + * → CO*	0.00	-1.06	/
26	bHCOO* + * → HCO* + O*	1.80	1.63	/
27*	CO(g) + OH* → mHCOO*	1.45	-1.01	0.10
28	HCO* + H* → H_2CO* + *	0.46	-0.47	0.02
29	H* + OH* → H_2O*	1.12	0.17	/
30	2OH* → H_2O* + O*	0.35	0.13	/
31	O* + H* → OH*	0.87	-0.69	/
32	H_2O(g) + * → H_2O*	0.00	-0.20	/
33	H_2CO(g) + 2* → HCO* + H*	0.85	0.35	0.13
34	H_2CO(g) + O* → H_2COO*	0.07	-0.99	0.03
35	H_2CO(g) + H* → H_2COH*	0.70	-0.54	0.41
36	HCOH* → H_2CO*	1.75	-0.42	0.01
37	t,cCOHOH* → c,cCOHOH*	0.73	0.53	/
38	c,cCOHOH* → COH* + OH*	0.59	-0.22	0.03
39	tCOOH* + * → COH* + O*	2.13	1.00	0.72
40	HCO* + * → H* + CO*	0.26	-0.66	/
41	COH* + * → H* + CO*	1.02	-0.75	0.18
42	HCO* + H* → HCOH*	1.15	-0.05	0.28
43^{vib}	CO_2(g) + 2* → CO* + O*	1.8	0.43	0.87
44	O_2(g) + * → O_2*	0.00	-0.21	/
45	O_2* + * → O* + O*	0.22	-2.40	/
46	O_2(g) + 2* → O* + O*	0.01	-2.61	0.01
47*	CH_2(g) + * → CH_2*	0.00	-2.87	/
48*	CH_3(g) + * → CH_3*	0.00	-1.28	/
49*	CH_2* + H* → CH_3* + *	0.61	-0.96	/
50*	CH_3* + H* → CH_4(g) + 2*	0.73	-1.20	/
51*	O(g) + * → O*	0.00	-6.55	/
52*	H(g) + * → H*	0.00	-3.58	/

53*	OH(g) + * → OH*	0.00	-3.75	/
54*	HCO(g) + * → HCO*	0.00	-1.73	/

3.3 Entropy values

The activation entropy is calculated as the difference in entropy between transition state (TS) and products. The reaction entropy is calculated as the difference in entropy between products and reactants. The entropy of adsorbates was assumed equal to zero as they will only have a very limited amount of freedom, i.e. most of their degrees of freedom (DoF) disappear upon adsorption. The entropy of gas phase species as function of temperature is calculated from[40]:

$$S(T) = S^\circ_{298K} - S_{trans}(298K) + S_{trans}(T)$$

Where S°_{298K} is the standard gas phase entropy, taken from the database of the National Institute of Standards and Technology (NIST).[41] $S_{trans}(T)$ is the entropy of the translational DoF at temperature T calculated as[40]:

$$S_{trans}(T) = R\ln\left(\frac{(2\pi m k_B T/h^2)^{3/2} V^0_{gas} e^{5/2}}{N_A}\right)$$

Where V^0_{gas} is the molar volume of the gas at its standard state, i.e. at a pressure of 1 bar and temperature T, m is the mass of the gas species and N_A is Avogadro's number. For reactions involving gas phase species, the TS was assumed to be a 2D gas, i.e. the TS is only weakly adsorbed on the surface and has lost one DoF, namely translation in the direction perpendicular to the surface. The entropy of a 2D gas is calculated as[35]:

$$S_{TS}(T) = S_{2Dgas}(T) = S^\circ_{298K} - S_{trans}(298K) + 2/3\, S_{trans}(T)$$

The only exception is dissociative adsorption. For this kind of reactions, we assumed that the TS is located at the surface and thus has zero entropy. This was done because a strong interaction with the catalyst is expected to be necessary for dissociation.

3.4 Impact of vibrationally excited species

Vibrationally excited species can be important in plasma catalysis, as explained in the Introduction. Their effect is implemented in the model by lowering the activation enthalpy for calculating the forward rate coefficient. First the rate coefficient for each vibrational level is calculated[29]:

$$k_{TST,\nu} = \frac{k_B T}{h} e^{\frac{\Delta S^\ddagger}{R}} e^{\frac{-(\Delta H^\ddagger - \alpha E_\nu)}{RT}}$$

where ν is the vibrational quantum number, E_ν is the energy of the vibrational level and α is a parameter that indicates how efficiently the energy of a certain vibrational excitation, i.e. normal mode, lowers the barrier (see further).

The new forward rate coefficient is then calculated as the sum of all rate coefficients for all vibrational levels, multiplied by their weight, *p(v)*, calculated from a Boltzmann distribution at a certain vibrational temperature, different from the gas temperature[29]:

$$k_{TST} = \sum_\nu p(\nu) k_{TST,\nu}$$

$$p(\nu) = \frac{e^{-\frac{E_\nu}{k_B T_{vib}}}}{\sum_\nu e^{-\frac{E_\nu}{k_B T_{vib}}}}$$

The α parameter is calculated by the Fridman – Macheret equation[42], which was also applied in previous works by Mehta et al.[26] and Engelmann et al.[28,29]:

$$\alpha = \frac{E_a^f}{E_a^f + E_a^b}$$

where E^f_a is the forward barrier and E^b_a is the barrier of the backward reaction. This formula is derived for a reaction of the type A + BC ⟶ AB + C in the gas phase and reproduces the most important characteristics of α that are observed experimentally: (1) the efficiency of vibrational energy to overcome the barrier is highest, i.e. α is close to 1, for strongly endothermic reactions that have an activation barrier close to the reaction enthalpy; (2) the efficiency of vibrational energy to overcome the barrier is lowest, i.e. α is close to 0, for strongly exothermic reactions without activation energy. A more detailed explanation and the derivation of the formula can be found in section 2.7.3 of the book 'Plasma Chemistry' by Alexander Fridman.[42]

Of course, the Fridman – Macheret model is very general and does not include any specific information on the reaction it is applied to (e.g., no dependence on specific vibrational modes). Nevertheless, it is used here, as there are, to the best of our knowledge, no values or other approximations for α reported in literature for the elementary reactions in the model. Hence, we evaluate the impact of varying the α parameter in this work (see below).

The backward rate coefficient is not altered, as the products encounter the same barrier because they are not vibrationally excited. Hence, the backward rate coefficient is still determined from the equilibrium constant and the forward rate coefficient calculated from the Eyring equation (see above).

To study the effect of excitation of the H_2 stretching mode, we adopted the vibrational levels from Poll et al.[43] The dependence of H_2 dissociation on Cu(111) on the vibrational DoF has been shown by Hammer et al.[44] For CO_2 we studied both the impact of excitation of the asymmetric stretching mode, ν_3, and excitation of the bending mode, ν_2. We assume that ν_3 has an impact on CO_2 dissociation, as this reaction was found to be promoted by both translational and vibrational excitation.[23] We assume that the asymmetric stretch also enhances HCOO* and COOH* formation, via the ER reaction of $CO_{2(g)}$ with H*. The basis of this assumption is the elongation of the C – O bond when HCOO* is formed from CO_2. This will require energy, which can be supplied by the asymmetric stretch mode because it overlaps with the reaction coordinate. The bending mode is often not considered, but was recently shown by Quan et al.,[25] to enhance HCOO* formation, as discussed in the Introduction. As this effect is attributed to the lower OCO angle in the TS, we assume that excitation of this mode also enhances COOH* formation, since HCOO* and COOH* have similar OCO angles. The vibrational levels of ν_3 are taken from Kozàk et al,[45] while for ν_2 the vibrational levels are calculated from the harmonic oscillator and the degeneracy of the mode is neglected for simplicity, because we only want to qualitatively study the impact of the different vibrational modes.

3.5 Plasma catalysis vs thermal catalysis

We used this model to simulate both thermal catalysis and plasma catalysis. For thermal catalysis, vibrational excitation is not included in the model and the gas phase pressures of the radicals and intermediates are equal to zero, i.e. considering only a CO_2 and H_2 pressure.

For plasma catalysis, the gas phase pressures of the radicals and intermediates are varied in a wide range, to evaluate their effect on the surface chemistry. The initial values are based on the model by De Bie et al.,[46] for plasma-driven hydrogenation of CO_2. In that paper, the H_2/CO_2 ratio was varied from 1:9 to 9:1, and the most abundant radicals were reported to be H, O, OH, HO_2, HCO, CH_3 and CH_2, while the most abundant products were CO, H_2O and CH_4. In addition, CH_2O, C_2H_6, O_2 and CH_3OH were formed to a lower extent. The mixing ratio did not drastically affect the densities of the formed products. Note that the reported CO_2 conversion was rather low, i.e. 2-7 %, certainly in comparison with the conversion predicted with the same model for plasma-based dry reforming of methane.[47] This was attributed to the much lower CH_2 and CH_3 radical densities. Additionally, the formation of HCO radicals was also found to limit the CO_2 conversion via the following reaction sequence:

$$CO_2 \rightarrow CO + O$$
$$CO + H + M \rightarrow HCO + M$$
$$HCO + O \rightarrow CO_2 + H$$

Furthermore, a lot of subsequent reactions were needed to form the desired reaction products, such as CH_3OH, making their overall production negligible. Hence, the authors concluded that, in general, a H_2/CO_2 plasma without catalyst was not suitable for the production of CH_3OH and other value-added chemicals, showing the need for a catalyst, as studied in this work.

It has to be noted that desorption of CO or radicals is not allowed in our model when the gas phase pressure of these species is zero, i.e. in thermal catalysis. Allowing desorption could result in a high TOF for these species and accumulation in the gas phase. However, as the gas phase pressures in the model are fixed, the pressure would remain zero. Consequently, the adsorption rate would remain zero, resulting in unrealistic production in the gas phase. In other words, production of these species would in reality result in faster adsorption, immediately compensating the desorption. When a gas phase pressure of these species is present, i.e. in the plasma, desorption is allowed since the adsorption rates will not be zero in this case. In case of thermal catalysis, this approach can be considered questionable for CO, as CO formation from H_2/CO_2 has been reported on a Cu catalyst.[2] However, in our model, based on the PED from Zhao et al.[31], small CO pressures in the gas phase resulted in fast CO adsorption and subsequent CO conversion, preventing significant CO yields. Hence, the assumption to not allow CO desorption in thermal catalysis is reasonable.

4. Results and Discussion

4.1 Thermal Catalysis

We first present results for thermal catalysis, as a benchmark for plasma catalysis. For this reason, we assume a gas phase pressure of 1 bar and temperature of 400 K. Indeed, plasma catalysis typically occurs in DBD plasma reactors, which operate at temperatures slightly above room temperature and pressures close to atmospheric pressure. In the Supporting Information (SI; section S.1), we present the TOF of the main products and the surface coverages (Figure S.1 (a) and (b), respectively), as function of the CO_2 content in the H_2/CO_2 gas mixture, and we compare our findings to literature and, if possible, improve our model to reach better agreement with literature, i.e., Models 1 and 2 in the SI.

As discussed in Section 2, three possible mechanisms are suggested in literature for CH_3OH formation from CO_2. The possible formation pathways predicted by our model are depicted in Figure 3. Hydrogenation steps are indicated with H* next to the arrow, possible rate-determining steps are shown in red. The formation of OH* and subsequent reaction to H_2O are omitted for clarity. We will briefly discuss these possible pathways, including the pathways which only make up a negligible

contribution to CH_3OH production, since they might become important under plasma conditions. We focus on the results of Model 2, and we refer to the SI for differences with Model 1.

The three pathways suggested in literature are also predicted by our model: a pathway through HCOO*, followed by HCOOH* or H_2COO* (formate path; green in Figure 3), a pathway through tCOOH* and t,tCOHOH* (hydrocarboxyl path; orange in Figure 3) and one through CO* (RWGS reaction), followed by CO* hydrogenation to HCO* or COH* (blue path in Figure 3). The rate of hydrogenation to COH* is seven orders of magnitude smaller than the rate of hydrogenation to HCO*. Nonetheless, an arrow from CO* to COH* was drawn in Figure 3, as this is responsible for almost 100% of COH* formation.

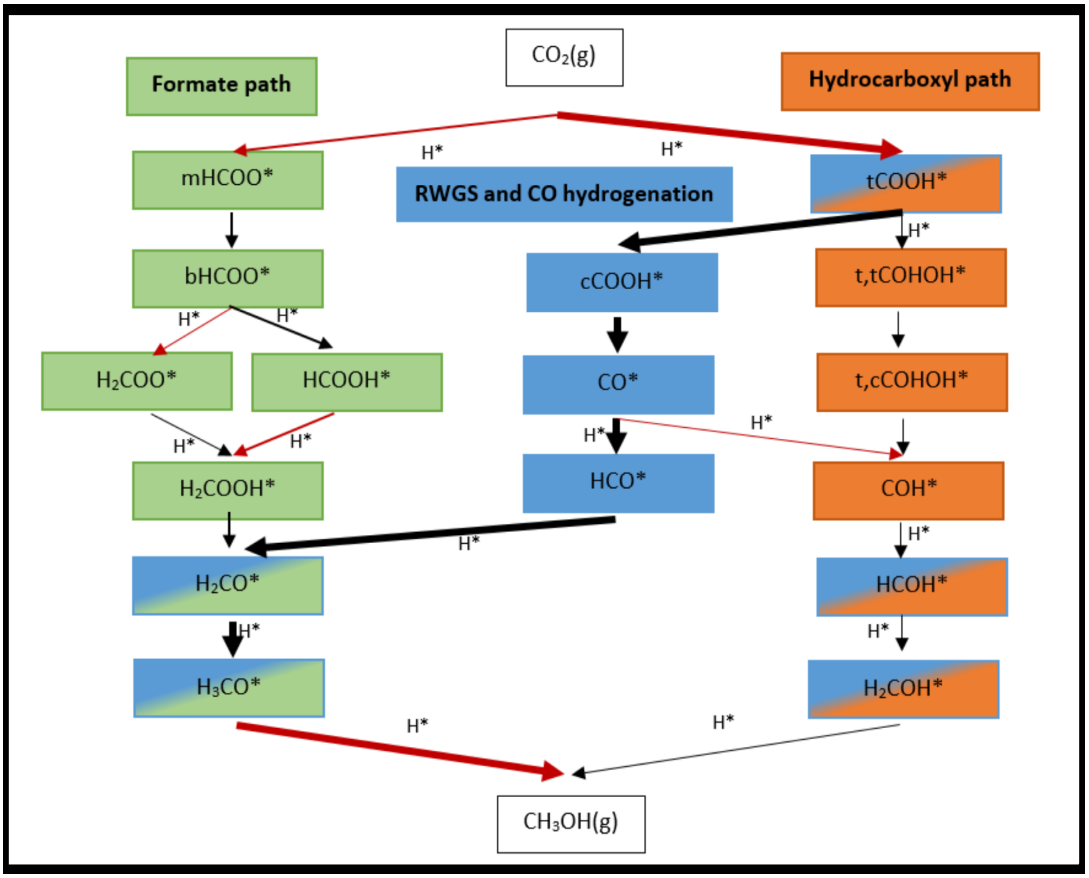

Figure 3: Possible pathways for CH_3OH formation predicted by our model for thermal catalysis. H* next to an arrow indicates a hydrogenation step. OH* and H_2O formation are omitted for clarity. The thickness of the arrows indicates the importance of each reaction (thickness is not proportional). Red arrows indicate the possible rate-determining steps. Intermediates that occur in two pathways have two colours.

To identify the main CH_3OH formation pathway, we need to compare the TOF of H_3CO* and H_2COH*. Hydrogenation of H_3CO* is four orders of magnitude faster than hydrogenation of H_2COH*. Hence, in our model both the RWGS pathway through COH* and the hydrocarboxyl pathway make a negligible contribution to CH_3OH formation in thermal catalysis.

To evaluate the importance of the formate path and the RWGS path through HCO*, we compared the rate of H_2COOH* dissociation into H_2CO* and OH* with the rate of HCO* hydrogenation, and we found that the latter is responsible for ca. 75% of H_2CO* formation. Thus, according to our model, CH_3OH is mainly produced via the RWGS pathway through HCO*.

The possible rate-determining step for the RWGS and CO* hydrogenation pathway is found to be tCOOH* formation from CO_2 (thick red arrow in upper right part of Figure 3). For the formate path, HCOO* formation, as well as HCOO*, HCOOH* and H_3CO* hydrogenation, are found to be possible rate-limiting steps (other red arrows in Figure 3). Hydrogenation of HCOO* is rate-determining for

the formate pathway through H_2COO*, while hydrogenation of HCOOH* and formation of HCOO* can both be rate-limiting for the formate pathway through HCOOH*, as the activation energy of both steps is similar. However, the formation of HCOO* is slightly more rate-limiting because of the entropy loss that accompanies this adsorption step.

The pathways predicted by our model are also reported in literature, but there is no consensus on which path is more important. Zhao et al.,[31] on which our reaction set is based, proposed the hydrocarboxyl path as main pathway for CH_3OH formation, but stated that this is only possible when H_2O* is present at the surface to facilitate the formation of COOH*. We find this to be unlikely since our model, both Models 1 and 2 (cf. SI), shows that tCOOH* formation could be possible without the presence of significant amounts of water at the surface. Furthermore, COOH* formation will lead to fast CO* formation and subsequent hydrogenation rather than formation of COH* through t,cCOHOH*. Zhao et al., recognized that COOH* formation will lead to fast CO* production, but hypothesized that CO* hydrogenation will not lead to CH_3OH formation, since the formation of HCO* is kinetically and thermodynamically unfavourable. However, they failed to recognize that subsequent HCO* hydrogenation has a low barrier and is thermodynamically favourable. Furthermore, the highest barrier in the proposed hydrocarboxyl path, i.e. 1.09 eV for COH* formation, is higher than any barrier in the CO* formation path. Other studies in literature often do not consider a COOH* intermediate. Consequently, they reported the formate path as the main path, either through H_2COO* or HCOOH*. Yang et al.[33,48] as well as Kattel et al.[34] also predicted that the RWGS and the formate path are the most important reaction channels on Cu, but predicted the formate path to be the most important channel towards CH_3OH. In their case, the CH_3OH production via CO* hydrogenation suffers from the low stability of the HCO* intermediate. This result was also reported by Kattel et al.[34] The fact that our model prefers CH_3OH formation via the RWGS path, is mostly due to the assumption that CO* cannot desorb from the surface, which was important because we worked with a fixed gas phase of CO_2/H_2. However, this assumption is not made in the plasma catalysis model, because it was not necessary, due to the presence of CO in the gas phase.

For these reasons, our model seems to sufficiently agree with previous research in order to further elucidate to mechanisms in plasma-catalytic CO_2 hydrogenation.

4.2 Plasma Catalysis: Effects of radicals and intermediates

Now that we described the possible mechanisms of thermal catalytic CH_3OH formation revealed by our model, we will discuss the results for plasma catalysis. To study the effects of the plasma, we used the adapted model (Model 2), since this model yielded better agreement with experiments and other theoretical studies. The results of the adapted thermal catalysis model will serve as benchmark for plasma catalysis. First, the effect of the radicals and intermediates formed in the plasma will be discussed, without considering the impact of vibrationally excited molecules. Subsequently, we will discuss the additional influence of vibrational excitation. If the conditions are not specified, the temperature is 400 K, the combined H_2/CO_2 pressure is 1 bar and the radical partial pressures are equal to those reported by De Bie et al.,[46] listed in Table 2. De Bie et al., modelled the plasma chemistry of a CO_2/H_2 DBD plasma and calculated the densities of the different plasma species. These densities are used as a first approximation of the gas phase composition upon introduction of a catalyst. Future models ideally consist of a combined plasma-surface chemistry model that simultaneously calculates gas phase and surface reactions, by introducing additional rate equations for the gas phase species. Such a model is however beyond the scope of this paper. To account for the influence of the catalyst on the plasma composition, the radical pressures are separately varied in section 4.2.2. This approach also allows to clearly discriminate the effect of the different species, which provides useful insight, and would be more difficult when all the gas phase pressures are interdependent.

The TOFs of the main products and the surface coverages are presented in the SI. Here we focus on the reaction pathways, to be compared with those of thermal catalysis.

4.2.1 Effects of a typical gas phase composition of a CO_2/H_2 plasma

Table 2: Pressures of plasma species used in the microkinetic model, based on De Bie et al.[46]

Plasma species	Pressure (bar)
CO	10^{-3}
H_2O	10^{-3}
H_2CO	10^{-6}
H	10^{-6}
O	10^{-7}
OH	10^{-9}
HCO	10^{-11}
CH_2	10^{-15}
CH_3	10^{-15}
CH_4	10^{-6}

We studied the effects of the radicals and the intermediates, generated by the plasma, by adding them to the model in a stepwise fashion. This approach was chosen to make it easier to discriminate the impact of the separate species, while still accounting for the fact that they will always occur together. We assume that the plasma-produced radicals can form products at the surface, and this is more effective than recombination in the gas phase, as the surface acts as a more effective 'third body', dissipating the high exothermicity of bond-forming reactions.

We added all radicals and intermediates listed in Table 2, but the effect of adding CO, O, H, OH and H_2O were much more pronounced than the effects of adding the other species, mainly due to their higher importance (pressures) in the plasma. Therefore, we will discuss here only the effects of adding CO, O, H, OH and H_2O, while the effects of adding H_2CO, HCO, CH_2, CH_3 and CH_4 are discussed in the SI (section S.2; cf Figures S.3 – S.6).

Figure S.3 in the SI illustrates the TOFs of the main products and the surface coverages, as a function of the CO_2 fraction in the H_2/CO_2 gas mixture, when CO, O, H, OH and H_2O are added to the gas phase, with the pressures defined by Table 2. It is clear that the CH_3OH TOF is predicted to be six to seven orders of magnitude higher than in thermal catalysis (cf. Figure S.3 vs Figure S.2 in SI). Such enhanced CH_3OH production was also reported by experiments.[13,16] Of course it should be noted that we only focus in our model on CH_3OH formation, and the formation of other oxygenates is not yet included.

Adsorption of plasma-generated H, O and CO is now the main source for H*, O* and CO*. The TOFs of these species are determined by their adsorption rates, equal to 5.68, 1.43×10^{-1} and 9.92×10^{-4} s^{-1}, respectively, at a 1:1 H_2/CO_2 ratio. Despite the fact that O* has the highest binding energy (i.e., 6.55 eV, compared to 3.58 eV for H*), and thus the highest barrier for desorption, the net rate of H* adsorption is the highest. Of course, H has a higher pressure than O in the gas phase (see Table 2) and adsorption of H is entropically less hindered. The TOF of CO* is lower, despite its pressure being three orders of magnitude higher than the pressure of H*. This is explained by the smaller binding energy of CO to the surface (i.e., 1.06 eV, compared to 3.58 eV for the binding energy of H*), leading

to a lower barrier for CO* desorption and thus a smaller net adsorption rate. Thus, CO* is no longer generated by surface reactions but by dissociation of CO_2 in the plasma and subsequent adsorption of CO. In the future we want to develop a combined plasma-surface chemistry model that simultaneously calculates gas phase and surface reactions.

The increased OH* and O* coverage lead to increased H_2O production. The influence of CO* is more complex. As illustrated in Figure 4, adsorbed CO* will react with H* to form HCO*. This intermediate can then be further hydrogenated to H_2CO*, H_3CO* and finally CH_3OH (red pathway in Figure 4). CO* hydrogenation to COH* is also possible, just as in thermal catalysis, but the rate is again negligible compared to hydrogenation to HCO*. Hence, it is not depicted in figure 4. In thermal catalysis, the formation of CO* and subsequent hydrogenation was the main pathway to produce CH_3OH. However, CO* was produced from a COOH* intermediate and the formation of this intermediate was found to be rate-limiting. Hence, CO generated by the plasma allows to bypass this rate-limiting step. We note that our previous assumption that CO* desorption is not possible in thermal catalysis, does not change this conclusion.

The rate of CO* hydrogenation is found to be 9.62×10^{-4} s^{-1}, at a 1:1 H_2/CO_2 ratio, and, as this step is rate-limiting, the CH_3OH TOF is expected to be the same. However, the TOF of CH_3OH is equal to 4.94×10^{-3} s^{-1} at this H_2/CO_2 ratio (Figure S.3(a)), hence a factor five higher. This means that there must be another pathway for H_3CO* production in plasma catalysis, that is almost one order of magnitude faster than the CO* hydrogenation pathway.

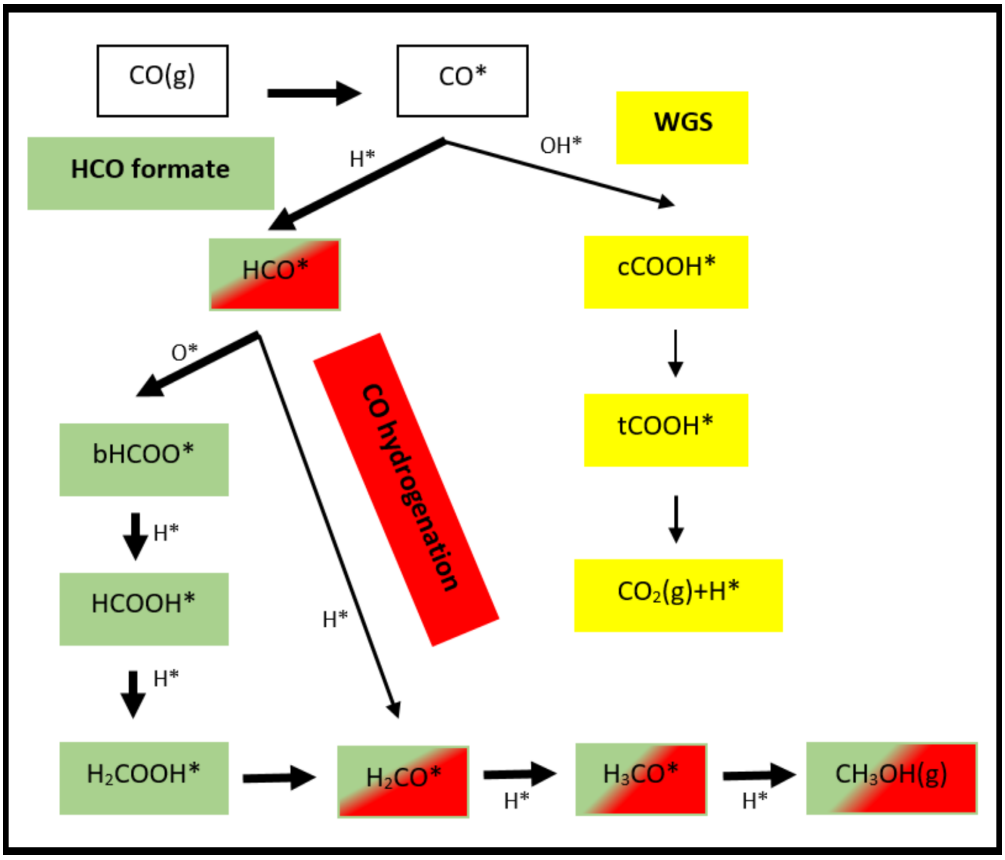

Figure 4: Mechanisms for CO consumption, leading to CH_3OH (green and red path) and CO_2 formation (yellow path). If H*, O* or OH* are involved in the reaction, they are depicted next to the arrow. The thickness of the arrows indicates the importance of the pathway (thickness is not proportional). OH* and H_2O formation are omitted for clarity. Intermediates that occur in two pathways have two colours.

Indeed, adding CO does not simply lead to CO hydrogenation. Firstly, the hydrogenation of HCO* is only responsible for ca. 6 % of HCO* loss. HCO* primarily reacts with O*, with a rate of 9.01×10^{-4} s^{-1} (again at a 1:1 H_2/CO_2 ratio), to form bHCOO*, which reacts further via the formate path into CH_3OH

(green pathway in Figure 4). This is also favourable, as this bypasses HCOO* formation from CO_2, which is rate-limiting in thermal catalysis. In thermal catalysis, the reaction with O* also occurs but at a much lower rate, so that it is not relevant for HCO* loss or bHCOO* formation, despite the fact that it is more favourable than hydrogenation. The reason for this is the low O* coverage in thermal catalysis. Since the O* coverage is enhanced in the case of plasma catalysis, the reaction will become more important. It will not only be the main loss reaction for HCO*, but it will also make up a significant contribution to bHCOO* formation.

An additional effect of the presence of CO is the reversal of the RWGS reaction. CO* will now react with OH* radicals to form cCOOH* (yellow pathway in Figure 4). The main reason for this is the higher OH* coverage. cCOOH* will react further to tCOOH*, which dissociates into H* and CO_2. This pathway is indicated as WGS in Figure 4, as it converts CO and OH* to CO_2 and H*, and thus H_2. In our model the OH* species is not formed from H_2O, but when this would be the case, the path converts CO and H_2O to CO_2 and H_2, hence it is called the WGS path. Only a negligible fraction of tCOOH* reacts to CH_3OH via the hydrocarboxyl pathway, similar as to thermal catalysis.

The formation of CO_2 from COOH* does not mean that CO_2 is no longer consumed by the catalyst. Indeed, CO_2 is still consumed through the formation of mHCOO*. mHCOO* then reacts further to CH_3OH via the formate pathway (green path in Figure 3 above). This pathway now goes through an HCOOH* intermediate, and the path through H_2COO* does no longer make a significant contribution to H_2COOH* formation. Thus, the formate path through HCOOH* is now the main pathway for CH_3OH formation, not only through HCOO* formation from CO_2, but also through HCOO* formation from CO via HCO*.

The higher mHCOO* TOF with respect to thermal catalysis, which is responsible for the much higher CH_3OH TOF (i.e., six-seven orders of magnitude; cf. Figure S.3 vs Figure S.2 in SI), is attributed to the increased H* coverage.

4.2.2 Variation of the partial pressures of the plasma species

To further study the influence of CO, O, H, OH and H_2O generated by the plasma, their partial pressure was varied in a wide range around the values reported by De Bie et al.[46] Indeed, the latter study simulated plasma conversion without catalyst, so the partial pressures of the plasma species are not necessarily the same as in plasma catalysis. Furthermore, we want to obtain a more generic understanding on the effect of plasma species on the TOFs, surface coverages and reaction pathways. The result is depicted in Figure 5, for varying the H partial pressure, while the partial pressures of the other plasma species are kept constant. Varying the other partial pressures yielded no additional insights.

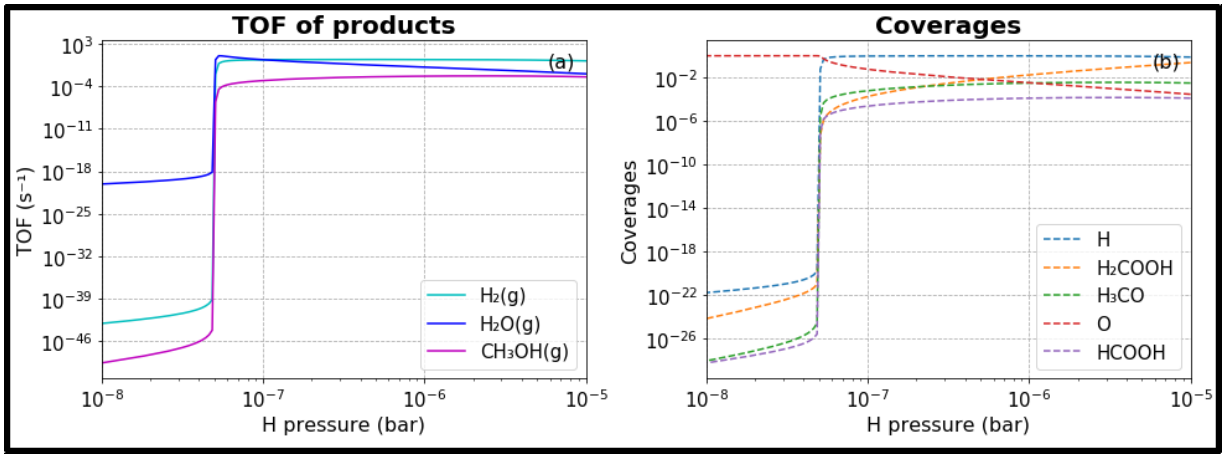

Figure 5: TOFs (a) and coverages (b) as a function of the H pressure, while the CO, O, OH and H_2O pressures are kept the same as in Table 2. When the H pressure is too low, the O* coverage becomes equal to 1, causing a significant drop in CH_3OH TOF.

When the H partial pressure is lower than ca. $5x10^{-8}$ bar, i.e., half of the O partial pressure (cf. Table 2), the surface is poisoned by O* (Figure 5 (b)). Indeed, O* is mainly consumed by reaction with H*, hence when the H* coverage is too low, this reaction becomes too slow to compensate for the O adsorption. This leads to O* poisoning, as no other reaction (including the formation of O_2, which has a relatively high activation barrier) is able to compensate for the fast adsorption. As can be seen in Figure 5 (a), the O* poisoning leads to a significant drop in the CH_3OH TOF. Thus, O* poisoning should be avoided. Higher H concentrations clear the surface of O* radicals, allowing more efficient hydrogenation reactions. Hence, there must be enough H* at the surface. Once this is the case, increasing the H pressure has no further effect (see Figure 5). In summary, our calculations suggest that the plasma composition should have a higher H than O partial pressure to ensure efficient CH_3OH formation.

4.2.3 Pathways to CH_3OH formation

A schematic overview of the main paths for plasma and thermal catalysis is depicted in Figure 6 (a) and (b). As mentioned in section 4.2.1, the main reason for the higher CH_3OH TOF is the enhanced production through the formate pathway via HCOOH* caused by the increased H* coverage.

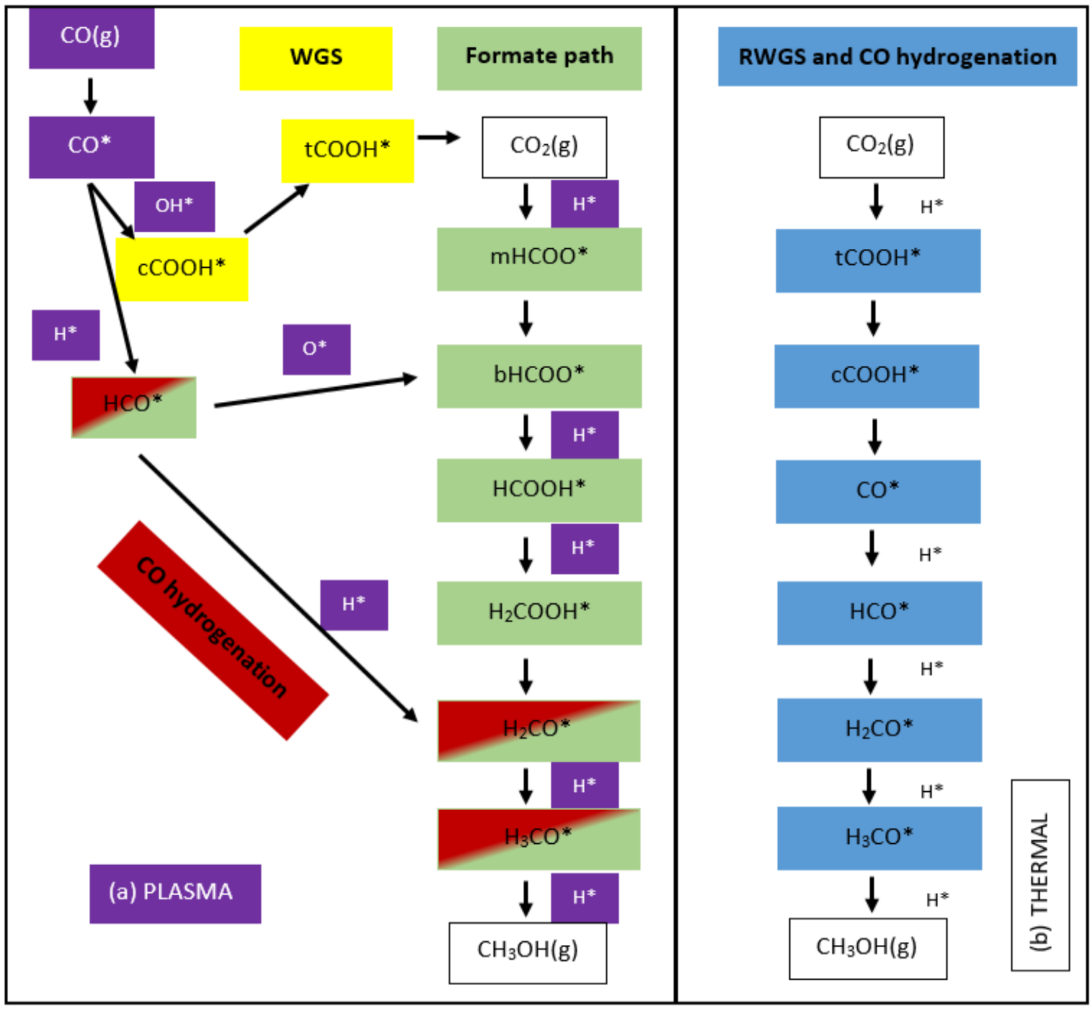

Figure 6: Overview of the most important pathways for CH_3OH formation in plasma catalysis (a) and thermal catalysis (b). In thermal catalysis, CH_3OH is mainly produced through the RWGS reaction and CO hydrogenation pathway (blue pathway). In plasma catalysis, CH_3OH is mainly produced via the formate path, both from CO_2 and CO (green pathway). CO is also converted to CH_3OH through hydrogenation (red pathway). Finally, CO is converted to CO_2 (yellow path). Species which are mainly supplied by the plasma are indicated in purple. OH* formation and H_2O formation were omitted for clarity. Intermediates that occur in two pathways have two colours.

Besides the formate pathway from CO_2, two pathways from CO contribute to CH_3OH formation, as explained in section 4.2.1, namely CO* hydrogenation (red path in Figure 4 and 6) and the formate path through HCO* (green path in Figure 4 and 6). We consider both paths favourable, as they avoid the formation of HCOO* directly from CO_2, which is found to be a bottleneck in the formate pathway. The HCO* hydrogenation pathway is one of the three alternative plasma bypasses proposed in section 2 (green dashed line in Figure 2). The other pathway proposed in Figure 2, namely CO*+OH* ® COOH* (yellow dashed line), will not play a direct role in increasing the CH_3OH production, according to our simulations. Although this reaction has a significant rate, it will lead to CO_2 formation (yellow path in Figure 4 and 6) rather than CH_3OH formation.

To the best of our knowledge, only Wang et al.,[16] have discussed some CH_3OH formation pathways in plasma catalysis. They suggested that both the formate path from CO_2 and CO hydrogenation are active paths, in accordance with our findings. They also considered the RWGS followed by CO hydrogenation path, but our calculations reveal that this path is not common in plasma catalysis. In summary, the fact that they suggested that CO formation in the gas phase and subsequent hydrogenation at the surface is responsible for the enhanced selectivity towards CH_3OH in plasma catalysis, correlates well with our model predictions.

The effects discussed above imply that both a high CO and H content in the plasma would be favourable for CH_3OH formation. However, a higher CO pressure always means a higher O, or OH, pressure, as CO in the plasma is formed through CO_2 dissociation, which also produces O atoms. The O or OH pressure should not be too high with respect to the H pressure, since this would result in O* poisoning of the catalyst surface. Consumption of O* through reaction with HCO* will not be able to compensate for the fast O* formation, as HCO* production will become slower due to a lower H* coverage. Thus, plasma conditions should be targeted to create a high CO and H content, while the O content should be minimized. A higher CO content can be realized by increasing the CO_2 fraction in the CO_2/H_2 mixture. We suggest that the CO_2 fraction should not exceed 90%, as De Bie et al., indicated that at higher CO_2 fractions the O content will be larger than the H content. A possible way to realize a high CO content without increasing the O content too much may be to selectively remove the O radicals from the plasma, e.g., by the combination with a membrane for O removal.[49]

To conclude, our model indicates that both CO_2 and CO can be the carbon source for CH_3OH production, and their partial pressures are therefore a determining factor. The O, OH and H pressures are also important, as they result in a higher surface coverage compared to thermal catalysis and this will determine the reactions CO undergoes.

4.3 Plasma Catalysis: Effects of vibrational excitation

As discussed in the introduction, vibrational excitation can lower the activation barrier of certain reactions. We only focus here on the effect of CO_2 vibrational excitation. Indeed, the impact of CO vibrational excitation is of limited interest, as CO dissociation does not occur on Cu, and the impact of vibrational excitation on reactions such as CO + OH* ®HCOO* is, to the best of our knowledge, unknown. Furthermore, the effect of H_2 vibrational excitation on the surface mechanisms or TOFs is negligible, when also plasma species are present, even when T_{vib} = 2000 K. Indeed, the H radicals from the gas phase will still be the main H source, as the enhanced rate coefficient of H_2 dissociative adsorption is still too small to make this rate higher than the H adsorption rate.

In the SI (section S.4), we discuss the impact of CO_2 vibrational excitation on the rate coefficients of dissociative adsorption (Figure S.8) and of HCOO* and COOH* formation (Figure S.9 and S.10). The gas temperature is always chosen to be 400 K in the calculations. As the vibrational temperature of the molecules depends on parameters like the power density, pressure, residence time and plasma composition, it was varied between 400 K (i.e., the vibrational DoF is in equilibrium with the translational DoF) and 2000 K. The vibrational temperature in a DBD is typically below 1000 K,[45] but

we chose to vary T_{vib} up to 2000 K to illustrate the potential of vibrational excitation. Furthermore, such vibrational temperatures (and higher) can be reached in a microwave or gliding arc plasma.[45]

In contrast to dissociative adsorption of CO_2 (and H_2), COOH* and HCOO* formation are more relevant to the model, as these steps are rate-limiting for the hydrocarboxyl and formate path, respectively. The calculated CH_3OH TOFs when including the excitation of the CO_2 bending mode (on top of the plasma-generated radicals and intermediates) are displayed in Figure 7 (blue line), for α_{HCOO*} = 0.43 and α_{COOH*} = 0.54 (i.e., Fridman-Macheret values; see section 3.4 above), in comparison with the TOF for thermal catalysis (Figure 7 (green line) and upon addition of only plasma-generated radicals and intermediates (Figure 7 (orange line). We ran the model including the effect of bending mode excitation, as this effect on HCOO* formation has been demonstrated by Quan et al., but also the excitation of the asymmetric stretch mode, as it is also likely to be kinetically important. We studied both excitations separately to be able to distinguish between both effects. In reality, there will be some degree of normal mode mixing. Furthermore, the effect of excitation of the two normal modes will qualitatively be the same but only differ in size. Hence, we will only discuss the impact on the TOF for excitation of the bending mode.

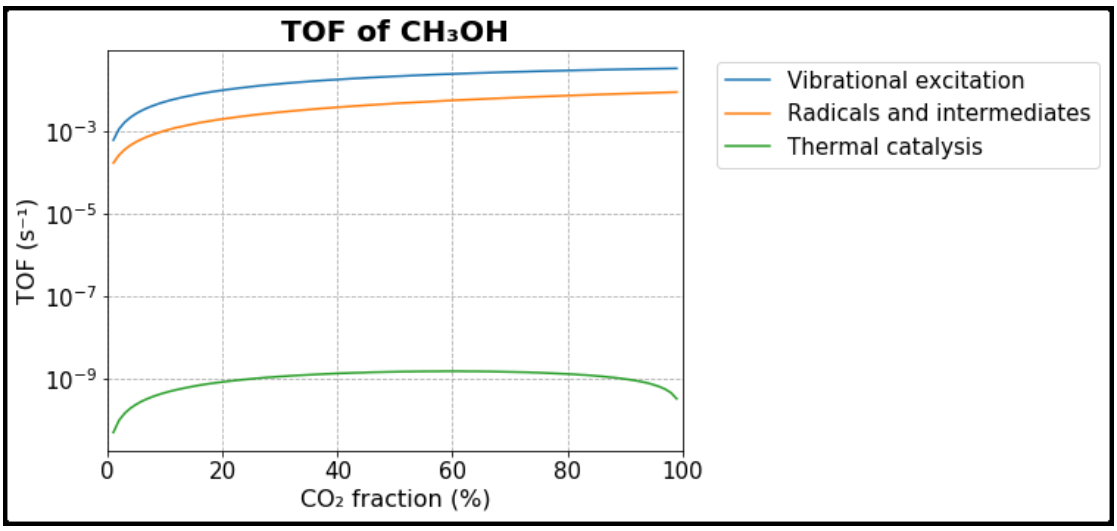

Figure7: TOF of CH_3OH in the case of thermal catalysis (green), and plasma catalysis upon addition of only plasma-generated radicals and intermediates (orange), and when also the effect of the excitation of the CO_2 bending mode is included (blue), as a function of the CO_2 content in the gas phase. (T_g = 400K, T_{vib}= 1000K)

As can be expected, the TOF of CH_3OH further increases by up to one order of magnitude compared to the results without vibrational excitation (but with plasma-generated radicals and intermediates; cf. Figure 7 (orange, blue)). This is due to a higher rate coefficient of HCOO* formation with one order of magnitude (Figure S.9), due to lowering of the activation barrier upon vibrational excitation of CO_2. This step was found to be a rate-limiting step for CH_3OH formation via the formate path, which is the most important path under plasma conditions.

The effect of vibrational excitation of CO_2 thus reinforces the impact of the plasma-generated radicals, that already gave rise to enhanced CH_3OH formation via the formate pathway. A high CO_2 content in the plasma is still favourable from the viewpoint of vibrational excitation, because excitation will speed up CO_2 consumption. Our model predicts however that in a DBD plasma the impact of vibrational excitation is limited, due to relatively low vibrational temperatures. Consequently, MW and GA plasmas, which can achieve higher vibrational temperatures, might be more favourable as they can further exploit this effect. However, such plasmas are more difficult to combine with catalyst, as they operate at higher gas temperature, possibly damaging the catalysts in case of in-plasma catalysis, and the lifetime of the vibrational states is most likely too short for post-plasma catalysis.

We note that besides T_{vib}, the impact of vibrational excitation strongly depends on the value of α, i.e. how efficient a certain vibrational mode is in supplying energy to the transition state. Hitherto, no accurate formulations of the α parameter exist, which is why we used to approximate Fridman-Macheret equation. Better understanding about the dynamics of the reactions studied above could provide more accurate α parameters, which are crucial for a more quantitative result. Possible ways to gain this understanding are DFT calculations, ensemble-based molecular simulations or molecular beam experiments.

4.4 Plasma Catalysis: Different pathways from thermal catalysis

In summary, we depict in Figure 8 the potential energy diagram of the pathways found to be active in plasma catalysis. The main pathway to CH_3OH in plasma catalysis is found to be the formate path through HCOOH* (green path in Figure 8). This path is the same as the one depicted in Figure 2 (orange path) but now goes through HCOOH* instead of H_2COO* as suggested by Zhao et al.[31]

Figure 8 also depicts the alternative plasma catalysis pathways to CH_3OH from CO_2 via CO, generated in the plasma, which are not present in thermal catalysis. Adsorbed CO* reacts with H* to HCO*, which in turn reacts with O* to HCOO* (light blue dashed path in Figure 8, which is faster than from CO_2 to HCOO*), followed by the formate path to CH_3OH. Adsorbed CO* also contributes to CH_3OH formation via a hydrogenation path (red dashed path in Figure 8). This is also suggested in Figure 2 (green path). Both CO hydrogenation and the CO contribution to the fomate path through HCO* are considered favourable, as they bypass the formation of COOH*, which is rate-limiting in thermal catalysis. Also, they will be relatively fast due to fast CO adsorption and slow CO desorption. Furthermore, our model reveals that vibrational excitation of CO_2 can further enhance CH_3OH formation as it lowers the barrier for HCOO* formation from CO_2 (purple path in Figure 8).

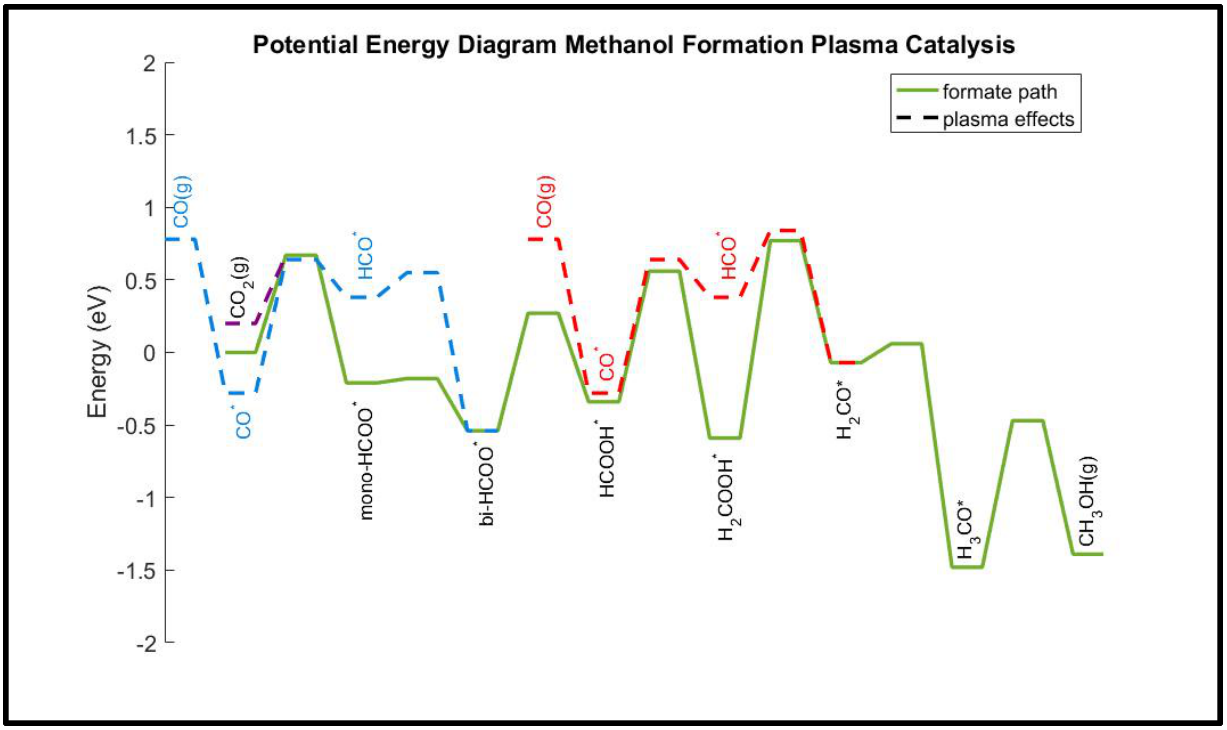

Figure 8: Overview of the pathways for CH_3OH synthesis in plasma catalysis. The purple dashed line indicates the lowering of the barrier due to vibrational excitation. The light blue dashed line indicates the contribution of CO to CH_3OH production via the formate path through HCO* and HCOO* formation. The red dashed line indicates the contribution of CO via CO hydrogenation through HCO* and H_2CO*.

5 Conclusion

The aim of this work is to elucidate the effect of plasma-generated radicals, intermediates and vibrationally excited species on the catalytic hydrogenation of CO_2 to CH_3OH on a Cu(111) surface, by means of a microkinetic model, based on the reaction set reported by Zhao et al.[31]

First, we used the model to study the mechanism of thermal catalytic CH_3OH formation, as a benchmark for plasma catalysis, and because there is no consensus on the main formation pathway in literature. Subsequently, we added gas phase pressures of plasma radicals and intermediates, to study their impact on the surface chemistry and TOF of CH_3OH. This resulted in a higher CH_3OH TOF by six to seven orders of magnitude, showing the potential of plasma-catalytic CO_2 hydrogenation into CH_3OH, in accordance with literature.

The main reason for the higher CH_3OH TOF in plasma catalysis is the higher production through the formate path via HCOOH* caused by the increased H* coverage. A significant contribution to CH_3OH formation through the formate path is made by CO through HCO* and subsequent HCOO* formation. Finally, CO hydrogenation via HCO* and H_2CO* also contributes to CH_3OH formation. Both paths through CO bypass the bottleneck in the formate path, namely HCOO* formation. This is in accordance with Wang et al.,[16] who observed significantly higher selectivity towards CH_3OH in plasma catalysis, which they suggested could be due to CO formation in the gas phase and the subsequent hydrogenation at the surface.

Furthermore, our model reveals that the H pressure should not be smaller than ca. half of the O pressure in the plasma, as this will cause O* poisoning, which in turn will result in very small product TOFs. Thus, plasma conditions should be targeted with a high CO and H content, as this is favourable for CH_3OH formation, while the O content should be minimized.

Finally, we investigated the impact of CO_2 vibrational excitation, and we found it to be highly dependent on the vibrational temperature and the efficiency by which vibrational energy is used to reach the transition state. Vibrational excitation of CO_2 further increases the CH_3OH TOF, as it enhances HCOO* formation, which is a rate-limiting step in the reaction mechanism. The effect is however limited to one order of magnitude, due to relatively low vibrational temperatures under typical plasma catalysis conditions, i.e. in a DBD plasma, and the high reactivity of the radicals.

In summary, we revealed the effects of plasma species on the catalytic CO_2 hydrogenation into CH_3OH on a Cu(111) catalyst. It should be realized, however, that the model is subject to uncertainties, due to the lack of information on the relevant reactions and rate coefficients. Hence, more and consistent DFT calculations are needed.

Supporting Information

The figures with the TOF and coverages are reported and discussed in the supplementary information. A section discussing the impact of using the experimental CO adsorption energy is also included, together with a detailed discussion of the impact of vibrational excitation on the rate coefficients of CO_2 dissociative adsoption, HCOO* and COOH* formation.

Acknowledgements

We acknowledge the financial support from the Fund for Scientific Research (FWO-Vlaanderen; grant ID 1114921N) and from the European Research Council (ERC) under the European Union's Horizon

2020 research and innovation programme (grant agreement No 810182 – SCOPE ERC Synergy project), as well as from the DOC-PRO3 and the TOP-BOF projects of the University of Antwerp.

References

(1) Álvarez, A.; Bansode, A.; Urakawa, A.; Bavykina, A. V.; Wezendonk, T. A.; Makkee, M.; Gascon, J.; Kapteijn, F. Challenges in the Greener Production of Formates/Formic Acid, Methanol, and DME by Heterogeneously Catalyzed CO2 Hydrogenation Processes. *Chem. Rev.* **2017**, *117* (14), 9804–9838.

(2) Porosoff, M. D.; Yan, B.; Chen, J. G. Catalytic Reduction of CO2 by H2 for Synthesis of CO, Methanol and Hydrocarbons: Challenges and Opportunities. *Energy Environ. Sci.* **2016**, *9* (1), 62–73.

(3) Olah, G. A.; Goeppert, A.; Prakash, G. K. S. *George A. Olah, Alain Goeppert, and G. K. Surya Prakash Beyond Oil and Gas: The Methanol Economy*; Wiley-VCH: Weinheim, 2009.

(4) Bowker, M. Methanol Synthesis from CO2 Hydrogenation. *ChemCatChem* **2019**, *11* (17), 4238–4246.

(5) Snoeckx, R.; Bogaerts, A. Plasma Technology – a Novel Solution for CO_2 Conversion? *Chem. Soc. Rev.* **2017**, *46*, 5805–5863.

(6) Bogaerts, A.; Neyts, E. C. Plasma Technology: An Emerging Technology for Energy Storage. *ACS Energy Lett.* **2018**, *3* (4), 1013–1027.

(7) Mehta, P.; Barboun, P.; Go, D. B.; Hicks, J. C.; Schneider, W. F. Catalysis Enabled by Plasma Activation of Strong Chemical Bonds: A Review. *ACS Energy Lett.* **2019**, *4* (5), 1115–1133.

(8) Neyts, E. C.; Ostrikov, K.; Sunkara, M. K.; Bogaerts, A. Plasma Catalysis: Synergistic Effects at the Nanoscale. *Chem. Rev.* **2015**, *115* (24), 13408–13446.

(9) Stangeland, K.; Li, H.; Yu, Z. Thermodynamic Analysis of Chemical and Phase Equilibria in CO2 Hydrogenation to Methanol, Dimethyl Ether, and Higher Alcohols. *Ind. Eng. Chem. Res.* **2018**, *57* (11), 4081–4094.

(10) Bos, M. J.; Brilman, D. W. F. A Novel Condensation Reactor for Efficient CO2 to Methanol Conversion for Storage of Renewable Electric Energy. *Chem. Eng. J.* **2015**, *278*, 527–532.

(11) van Bennekom, J. G.; Venderbosch, R. H.; Winkelman, J. G. M.; Wilbers, E.; Assink, D.; Lemmens, K. P. J.; Heeres, H. J. Methanol Synthesis beyond Chemical Equilibrium. *Chem. Eng. Sci.* **2013**, *87*, 204–208.

(12) Bogaerts, A.; Tu, X.; Whitehead, J. C.; Centi, G.; Lefferts, L.; Guaitella, O.; Azzolina-Jury, F.; Kim, H.-H.; Murphy, A. B.; Schneider, W. F.; et al. The 2020 Plasma Catalysis Roadmap. *J. Phys. D. Appl. Phys.* **2020**, *53*.

(13) Eliasson, B.; Kogelschatz, U.; Xue, B.; Zhou, L. M. Hydrogenation of Carbon Dioxide to Methanol with a Discharge-Activated Catalyst. *Ind. Eng. Chem. Res.* **1998**, *37* (8), 3350–3357.

(14) Zeng, Y.; Tu, X. Plasma-Catalytic CO2 Hydrogenation at Low Temperatures. *IEEE Trans. Plasma Sci.* **2016**, *44* (4), 405–411.

(15) Parastaev, A.; Hoeben, W. F. L. M.; van Heesch, B. E. J. M.; Kosinov, N.; Hensen, E. J. M. Temperature-Programmed Plasma Surface Reaction: An Approach to Determine Plasma-Catalytic Performance. *Appl. Catal. B Environ.* **2018**, *239* (August), 168–177.

(16) Wang, L.; Yi, Y.; Guo, H.; Tu, X. Atmospheric Pressure and Room Temperature Synthesis of Methanol through Plasma-Catalytic Hydrogenation of CO2. *ACS Catal.* **2018**, *8* (1), 90–100.

(17) Liu, S.; Winter, L. R.; Chen, J. G. Review of Plasma-Assisted Catalysis for Selective Generation of Oxygenates from CO2 and CH4. *ACS Catal.* **2020**, *10* (4), 2855–2871.

(18) Bal, K. M.; Huygh, S.; Bogaerts, A.; Neyts, E. C. Effect of Plasma-Induced Surface Charging on Catalytic Processes: Application to CO2 Activation. *Plasma Sources Sci. Technol.* **2018**, *27* (2).

(19) Jafarzadeh, A.; Bal, K. M.; Bogaerts, A.; Neyts, E. C. CO2 Activation on TiO2-Supported Cu5 and Ni5 Nanoclusters: Effect of Plasma-Induced Surface Charging. *J. Phys. Chem. C* **2019**, *123* (11),

6516–6525.

(20) Jafarzadeh, A.; Bal, K. M.; Bogaerts, A.; Neyts, E. C. Activation of CO2 on Copper Surfaces: The Synergy between Electric Field, Surface Morphology, and Excess Electrons. *J. Phys. Chem. C* **2020**, *124* (12), 6747–6755.

(21) Bal, K. M.; Bogaerts, A.; Neyts, E. C. Ensemble-Based Molecular Simulation of Chemical Reactions under Vibrational Nonequilibrium. *J. Phys. Chem. Lett.* **2020**, *11* (2), 401–406.

(22) Juurlink, L. B. F.; Killelea, D. R.; Utz, A. L. State-Resolved Probes of Methane Dissociation Dynamics. *Prog. Surf. Sci.* **2009**, *84* (3–4), 69–134.

(23) Jiang, B.; Guo, H. Communication: Enhanced Dissociative Chemisorption of CO2 via Vibrational Excitation. *J. Chem. Phys.* **2016**, *144* (9).

(24) Farjamnia, A.; Jackson, B. The Dissociative Chemisorption of CO2 on Ni(100): A Quantum Dynamics Study. *J. Chem. Phys.* **2017**, *146* (7).

(25) Quan, J.; Muttaqien, F.; Kondo, T.; Kozarashi, T.; Mogi, T.; Imabayashi, T.; Hamamoto, Y.; Inagaki, K.; Hamada, I.; Morikawa, Y.; et al. Vibration-Driven Reaction of CO2 on Cu Surfaces via Eley–Rideal-Type Mechanism. *Nat. Chem.* **2019**, *11* (8), 722–729.

(26) Mehta, P.; Barboun, P.; Herrera, F. A.; Kim, J.; Rumbach, P.; Go, D. B.; Hicks, J. C.; Schneider, W. F. Overcoming Ammonia Synthesis Scaling Relations with Plasma-Enabled Catalysis. *Nat. Catal.* **2018**, *1* (4), 269–275.

(27) Mehta, P.; Barboun, P. M.; Engelmann, Y.; Go, D. B.; Bogaerts, A.; Schneider, W. F.; Hicks, J. C. Plasma-Catalytic Ammonia Synthesis Beyond the Equilibrium Limit. *ACS Catal.* **2020**, No. 2, 1–24.

(28) Engelmann, Y.; van 't Veer, K.; Gorbanev, Y.; Neyts, E. C.; Schneider, W. F.; Bogaerts, A. Plasma Catalysis for Ammonia Synthesis: Contributions of Eley-Rideal Reactions. *(submitted)*.

(29) Engelmann, Y.; Mehta, P.; Neyts, E. C.; Schneider, W. F.; Bogaerts, A. Predicted Influence of Plasma Activation on Nonoxidative Coupling of Methane on Transition Metal Catalysts. *ACS Sustain. Chem. Eng.* **2020**, *8* (15), 6043–6054.

(30) Grabow, L. C.; Mavrikakis, M. Mechanism of Methanol Synthesis on Cu through CO2 and CO Hydrogenation. *ACS Catal.* **2011**, *1* (4), 365–384.

(31) Zhao, Y. F.; Yang, Y.; Mims, C.; Peden, C. H. F.; Li, J.; Mei, D. Insight into Methanol Synthesis from CO2 Hydrogenation on Cu(1 1 1): Complex Reaction Network and the Effects of H2O. *J. Catal.* **2011**, *281* (2), 199–211.

(32) CHINCHEN, G. C.; DENNY, P. J.; JENNINGS, J. R.; SPENCER, M. S.; WAUGH, K. C. ChemInform Abstract: Synthesis of Methanol. Part 1. Catalysts and Kinetics. *ChemInform* **1988**, *19* (22), 1–65.

(33) Yang, Y.; Evans, J.; Rodriguez, J. A.; White, M. G.; Liu, P. Fundamental Studies of Methanol Synthesis from CO2 Hydrogenation on Cu(111), Cu Clusters, and Cu/ZnO(0001). *Phys. Chem. Chem. Phys.* **2010**, *12* (33), 9909–9917.

(34) Kattel, S.; Ramirez, P.; Chen, J. G.; Rodriguez, J. A.; Liu, P. Active Sites for CO2 Hydrogenation to Methanol on Cu/ZnO Catalysts. *Science (80-.).* **2017**, *355*, 1296–1299.

(35) Yang, Y.; Mims, C. A.; Mei, D. H.; Peden, C. H. F.; Campbell, C. T. Mechanistic Studies of Methanol Synthesis over Cu from CO/CO 2/H2/H2O Mixtures: The Source of C in Methanol and the Role of Water. *J. Catal.* **2013**, *298*, 10–17.

(36) Studt, F.; Behrens, M.; Kunkes, E. L.; Thomas, N.; Zander, S.; Tarasov, A.; Schumann, J.; Frei, E.; Varley, J. B.; Abild-Pedersen, F.; et al. The Mechanism of CO and CO2 Hydrogenation to Methanol over Cu-Based Catalysts. *ChemCatChem* **2015**, *7* (7), 1105–1111.

(37) Xu, L.; Lin, J.; Bai, Y.; Mavrikakis, M. Atomic and Molecular Adsorption on Cu(111). *Top. Catal.* **2018**, *61* (9–11), 736–750.

(38) Hummelshøj, J. S.; Abild-Pedersen, F.; Studt, F.; Bligaard, T.; Nørskov, J. K. CatApp: A Web Application for Surface Chemistry and Heterogeneous Catalysis. *Angew. Chemie - Int. Ed.* **2012**, *51* (1), 272–274.

(39) Zhao, Z. J.; Li, Z.; Cui, Y.; Zhu, H.; Schneider, W. F.; Delgass, W. N.; Ribeiro, F.; Greeley, J.

Importance of Metal-Oxide Interfaces in Heterogeneous Catalysis: A Combined DFT, Microkinetic, and Experimental Study of Water-Gas Shift on Au/MgO. *J. Catal.* **2017**, *345*, 157–169.

(40) Campbell, C. T.; Sprowl, L. H.; Árnadóttir, L. Equilibrium Constants and Rate Constants for Adsorbates: Two-Dimensional (2D) Ideal Gas, 2D Ideal Lattice Gas, and Ideal Hindered Translator Models. *J. Phys. Chem. C* **2016**, *120* (19), 10283–10297.

(41) Johnson III, R. D. NIST Computational Chemistry Comparison and Benchmark Database NIST Standard Reference Database Number 101.

(42) Fridman, A. *Plasma Chemistry*; Cambridge University Press: Cambridge, 2008.

(43) Poll, J. D.; Karl, G. On the Vibrational Frequencies of the Hydrogen Molecule. *Can. J. Phys.* **1966**, *44* (7), 1467–1477.

(44) Hammer, B.; Schleffer, M.; Jacobsen, K.; Nørskov, J. K. Multidimensional Potential Energy Surface for H2 Dissociation over Cu (111). *Phys. Rev. Lett.* **1994**, *73* (10), 1400–1403.

(45) Kozák, T.; Bogaerts, A. Splitting of CO2 by Vibrational Excitation in Non-Equilibrium Plasmas: A Reaction Kinetics Model. *Plasma Sources Sci. Technol.* **2014**, *23* (4), 045004.

(46) De Bie, C.; Van Dijk, J.; Bogaerts, A. CO2 Hydrogenation in a Dielectric Barrier Discharge Plasma Revealed. *J. Phys. Chem. C* **2016**, *120* (44), 25210–25224.

(47) De Bie, C.; Van Dijk, J.; Bogaerts, A. The Dominant Pathways for the Conversion of Methane into Oxygenates and Syngas in an Atmospheric Pressure Dielectric Barrier Discharge. *J. Phys. Chem. C* **2015**, *119* (39), 22331–22350.

(48) Yang, Y.; White, M. G.; Liu, P. Theoretical Study of Methanol Synthesis from CO 2 Hydrogenation on Metal-Doped Cu(111) Surfaces. *J. Phys. Chem. C* **2012**, *116* (1), 248–256.

(49) Mori, S.; Matsuura, N.; Tun, L. L.; Suzuki, M. Direct Synthesis of Carbon Nanotubes from Only CO2 by a Hybrid Reactor of Dielectric Barrier Discharge and Solid Oxide Electrolyser Cell. *Plasma Chem. Plasma Process.* **2016**, *36* (1), 231–239.

TOC Graphic